Research On Abnormal Detection Of Transmission Lines In High-risk Areas On The Distribution Network Side Under Extreme Weather Conditions

*Anjiang Liu, Youzhuo Zheng, Di Weng, Hengrong Zhang, and Xinhao Li

Electric Power Research Institute, Guizhou Power Grid Co., Ltd, Guiyang, 550002, China

Corresponding author. E-mail: leeli@hust.edu.cn

Received May 4, 2026; accepted July 12, 2026

This paper presents an integrated electric-gas energy system fault recovery method based on bidirectional coupled devices. Simulation examples of an IEEE 13-node electric system and a 6-node natural gas system are used to validate the effectiveness of the method. YALMIP is used to model the simulations in the MATLAB environment, while CPLEX is used to solve the optimization issue. Three recovery strategies are compared under the system failure scenarios: independent failure recovery, failure recovery with GFT coupling only, and failure recovery taking into account both GFT and P2G coupling. The power and natural gas systems are bi-directionally coupled through one GFT and one P2G device. The outcomes demonstrate that the recovery strategy that incorporates the consideration of two-way coupled devices can greatly enhance the recovery of natural gas and electricity loads. Scenario 3' s total recovery is 41,488.12, which is 66.64% and 55.94% of Scenario 1 and Scenario 2' s respective recoveries. Through a detailed analysis of the changes in network topology and the output of energy conversion equipment during the recovery process, the resilience and effectiveness of the method presented in this study under various fault scenarios are confirmed.

Keywords: integrated electric-gas energy system, fault recovery, two-way coupling, GFT, P2G, supply reliability.

http://dx.doi.org/110.6180/jase.202611_34.030

1. Introduction

The trend of connecting the development of the natural gas and electric power systems has emerged due to the shift in the energy structure and the steady rise in the share of clean energy. Reducing greenhouse gas emissions, increasing energy supply reliability, and increasing energy utilization efficiency are all potential benefits of this type of Electric-Gas Integrated Energy System (EGIES) [1, 2]. In actuality, though, EGIES still has a lot of difficulties, particularly when it comes to handling system malfunctions and achieving quick recovery. A popular topic in current research is how to use distributed energy supplies and connected devices within the system for effective fault recovery [3].

An integrated electric-gas energy system uses linked equipment to convert energy in both directions between the networks for natural gas and electricity. Power-to-Gas (P2G) and Gas Fired Turbines (GFT) are common coupling devices. While P2G devices may convert excess energy back to natural gas and are useful for regulating the natural gas system, GFT devices can convert natural gas into electricity and are appropriate for power system support [4, 5]. The secret to raising EGIES' overall reliability in the event of a system failure is figuring out how to coordinate the operation of these linked devices to quickly restore the natural gas and electric systems [6].

The possibility for numerous connected devices functioning in concert has not been adequately examined in recent studies on fault recovery strategies for integrated electric-gas energy systems. These studies have primarily focused on unidirectional coupling or the employment of basic energy conversion devices [7]. Furthermore, after a fault, there are fewer dynamic evaluations of the topological changes that occur during the recovery phase in natural gas and electricity networks. By coordinating the operation of GFT and P2G devices, a fault recovery method based on bidirectional coupled devices is proposed in this study with the goal of improving the recovery efficiency and reliability of the systems and optimizing the recovery paths and resource allocation of power and natural gas systems [8, 9].

Extreme weather events may induce transmission line abnormalities and component outages, thereby causing power supply interruptions and increasing operational stress on distribution systems. In such circumstances, integrated electric-gas energy systems provide additional operational flexibility through coordinated electricity-gas interactions and energy conversion mechanisms.

This paper presents a novel optimization technique for cooperative fault recovery of two-way coupled devices. Detailed simulation experiments are used to validate the effectiveness of this technique in enhancing the resilience and energy supply reliability of integrated electric-gas energy systems (EGIES). The study' s findings offer fresh perspectives and technical backing for EGIES' s upcoming failure recovery plans.

2. The kind and quantity of points in a spatiotemporal configuration

The kind and quantity of configuration points affect the dynamic pipe flow PDE model' s accuracy and efficiency for gas networks using STOC [10]. The STOC-based dynamic pipe flow modelling framework transforms the transient natural gas flow process into an optimal control problem defined over both temporal and spatial domains. To improve computational tractability, the continuous state and control trajectories are represented by a finite number of spatiotemporal configuration points. Table 1 [11] illustrates the primary distinctions between the three often utilized configuration point types: Legendre-Gauss (LG), Legendre Gauss-Radau (LGR), and Legendre-Gauss-Labotto (LGL).

Table 1 defines (L_K) as the Legendre polynomial of order (K). The solution accuracy of LG, LGR, and LGL configuration points was comprehensively evaluated in [12], which showed that LGL points are slightly less accurate than LG and LGR points, while the STOC validation in [13] confirmed the efficiency and superiority of using LGR discretization in time and LG discretization in space. The deterministic N-1 contingency criterion is adopted to represent the loss of a single critical component while maintaining the secure operation of the remaining interconnected infrastructures. The considered contingency scenarios establish the basis for evaluating system resilience and determining appropriate corrective recovery actions following fault occurrences.

Though the validation examples in the literature [14] focus on low-dimensional nonlinear control problems, for high-dimensional nonlinear natural gas networks, the spatial endpoints of the pipeline must be included in the configuration points in order to introduce the state variables of f (x, t) at the pipeline endpoints to participate in the optimization, given that the flow equilibrium conditions at the network' s nodes must be satisfied. In light of the aforementioned factors, this study uses LGR configuration points for the gas network' s state variables in the temporal domain and LGL configuration points in the geographical domain. The proposed STOC formulation provides an efficient approximation of the dynamic gas flow process, practical integrated electric-gas systems may exhibit strongly nonlinear transient behaviors during fault recovery and rapid load transitions. The adopted LGR configuration point discretization provides an efficient approximation of the dynamic behaviour of integrated electricity-gas systems while maintaining a relatively low computational burden. Owing to the spectral properties of the LGR scheme, the discretization approach can effectively capture transient state variations and preserve the consistency of dynamic state representations during fault recovery processes.

3. Model of optimal energy flow with safety constraints

This section develops a safety-constrained optimal energy flow model to determine corrective control strategies for N-1 faults in the integrated electricity-gas system based on dynamic gas pipeline flow constraints. The model utilizes the post-fault energy flow state as the reference operating point and minimizes corrective control costs subject to electricity-gas coupling, natural gas system, and power system constraints.

3.1. Constraints of the natural gas system

The safety-constrained optimal energy flow model incorporates dynamic pipe flow, node flow balance, pipeline-node connectivity, safety limits, and state variable boundary conditions of the natural gas system. According to the proposed STOC-based dynamic pipe flow model, the transient gas flow process satisfies the constraints at the defined spatiotemporal configuration points.

Table 1. Dissimilarities among the three types of configuration points

Types of	Configuration method	Node distribution
LG	Gauss orthogonal arrangement	’s zero point (finding nodes inside the domain)
LGR	Radau orthogonal arrangement	’s zero point (including -1)
LGL	Labotto orthogonal arrangement	-1.,+1 zero point (including ±1)

$$\begin{cases} \frac{1}{\Delta t_{mn} A} \sum_{k=0}^{N_m^{mm}} \alpha_{j,k}^t f_{mn,ik} \\ \qquad + \frac{1}{\Delta x_{mn}} \sum_{k=0}^{N_m^{mn}+1} \alpha_{i,k}^x p_{mn,kj} + \frac{\lambda \bar{v}_{mn} f_{mn,jj}}{2DA} = 0 \\ \frac{1}{\Delta t_{mn}} \sum_{k=0}^{N_n^{m+}} \alpha_{j,k}^t p_{mn,ik} \\ \qquad + \frac{c^2}{\Delta x_{mn} A} \sum_{k=0}^{N_{mm}^{mm}+1} \alpha_{i,k}^x f_{mn,kj} = 0 \quad \forall m,n \in \gamma \end{cases} \tag{1}$$

In the pipe mn, at the spatiotemporal configuration points (x_{i,t_j}), are the values of the mass flow rate and gas pressure, respectively, represented by $f_{mn,i,k}$and$p_{mn,k,j}$,$i = 0,\ldots,N_{x,nm}+1; j = 0,1,\ldots,N_{t,nm}$.

At the natural gas system’ s node, the flow balance equation is provided by

$$f_{\mathrm{S}m,j} - f_{\mathrm{L}m,j} - f_{\mathrm{T}m,j} + \sum_{n\in\delta_{\mathrm{in}}(m)} f_{nm,(N_x^{nm}+1)j} - \sum_{n\in\delta_{\mathrm{out}}(m)} f_{mn,0j} + \sum_{n\in\gamma_{\mathrm{in}}(m)} f_{\mathrm{C}nm,(N_x^{nm}+1)j} - \sum_{n\in\gamma_{\mathrm{out}}(m)} f_{\mathrm{C}mn,0j} = 0 \quad \forall m \in \gamma \tag{2}$$

where $\Omega_{in}(m)$ and $\Omega_{out}(m)$ are the set of nodes connected to the common pipeline flowing into and out of node m, respectively; $f_{S,m,j}, f_{L,m,j}, f_{T,m,j}$ is the value of the mass flow rate of the gas source at node m, the mass flow rate of the gas unit inlet, and the mass flow rate of the other gas loads at the time configuration point t_j.

The mass flow rates at the time configuration point t_j are t_j at the gas network pipeline’ s exit (m) and$f_{nm,N_{x,mn}+1,j}$at the pipeline’ s input (mn);At time configuration point t_j, the mass flow rates at the outlet m of the compressor pipeline nm and the inlet m of the compressor pipeline mn are t_j and $f_{mn,0,j}$, respectively. The set of nodes connected to the compressor pipeline flowing into and out of node m is represented by t_j and $f_{nm,N_{x,mn}+1,j}$.

The natural gas system’ s pipeline and node pressures meet the

$$p_{mn,0,j} = p_{m,j} = p_{nm,N_{x,nm}+1,j}, \quad m \in \Omega_{in}(m), n \in \Omega_{out}(m) \tag{3}$$

At time configuration point$\Omega_{g,in}(m)$, the pressure at node m is represented by$\Omega_{g,out}(m)$. The natural gas system variables must satisfy the following safety limit constraints:

$$\begin{cases} \underline{p}_{mn} \le p_{mn,ij} \le \bar{p}_{mn} \\ \underline{f}_{mn} \le f_{mn,ij} \le \bar{f}_{mn} \\ \underline{f}_{\mathrm{S}m} \le f_{\mathrm{S}m}^{\mathrm{set}} \le \bar{f}_{\mathrm{S}m} \quad \forall m,n \in \gamma \\ \underline{f}_{\mathrm{L}m} \le f_{\mathrm{L}m}^{\mathrm{set}} \le \bar{f}_{\mathrm{L}m}^0 \\ \underline{f}_{\mathrm{T}m} \le f_{\mathrm{T}m}^{\mathrm{set}} \le \bar{f}_{\mathrm{T}m} \end{cases} \tag{4}$$

where the pipe mn’s working pressure has upper and lower bounds of $i = 0,\ldots,N_x^{mn}; j = 0,1\ldots N_t^{mn}$, $\bar{p}_{mn}$, and $\underline{p}_{mn}$, respectively.

The maximum and minimum gas flow rates that the pipe mn can supply are $\bar{f}_{mn}$ and $\underline{f}_{mn}$, respectively; the maximum and minimum gas flow rates at node m are $\bar{f}_{\mathrm{S}m}$ and $\underline{f}_{\mathrm{S}m}$.

The lower bound of node m’s load flow is $\underline{f}_{\mathrm{L}m}$. The upper and lower bounds of the gas unit’s adjustable intake at node m are $\underline{f}_{\mathrm{T}m}$ and $\bar{f}_{\mathrm{T}m}$. The lower and upper bounds of the gas unit’s adjustable intake at node m have to be met for node m. It is necessary to fulfill the following requirements for node m, $\forall m,n \in \gamma$.

$$\begin{cases} p_{mn,ij} = c^2 \rho_{mn,jj} \\ p_{mn,i0} = p_{mn,i}^0 \quad \forall i = 0,\cdots,N_x^{mn}+1 \\ f_{mn,i0} = f_{mn,i}^0 \quad \forall i = 0,\cdots,N_x^{mn}+1 \\ f_{\mathrm{S}m,0} = f_{\mathrm{S}m}^0 \quad f_{\mathrm{S}m,j} = f_{\mathrm{S}m}^{\mathrm{set}} \quad \forall j = 1,\cdots,N_t^{mn} \\ f_{\mathrm{L}m,0} = f_{\mathrm{L}m}^0 \quad f_{\mathrm{L}m,j} = f_{\mathrm{L}m}^{\mathrm{set}} \quad \forall j = 1,\cdots,N_t^{mn} \\ f_{\mathrm{T}m,0} = f_{\mathrm{T}m}^0 \quad f_{\mathrm{T}m,j} = f_{\mathrm{T}m}^{\mathrm{set}} \quad \forall j = 1,\cdots,N_t^{mn} \end{cases} \tag{5}$$

where $f_{mn,i}^0$ and $p_{mn,i}^0$ are the values of the pipe mn at the configuration point ξ_i at the initial moment, respectively; and $p_{mn,ij}$ is the value of the gas density in the pipe mn at the spatio-temporal configuration point (ξ_i, τ_j);

The initial moment’s mass flow rates for the node m gas source, gas load, and gas unit intake are $f_{\mathrm{S}m,0}, f_{\mathrm{L}m,0}, f_{\mathrm{T}m,0}$; the corrective control strategy’s mass flow rates for the node m gas source, gas load, and gas unit intake are $f_{Sm}^{\rm set}, f_{\rm Lm}^{\rm set}, f_{\rm Tm}^{\rm set}$.

The state equation between gas pressure and density is represented by the first equation in Eq. (5); the boundary conditions that the pipeline mn' s state variables (pressure and mass flow rate) satisfy at the initial moment $t_j$are represented by the second and third equations. The AC current constraints are reformulated using second-order cone programming to obtain a convex representation of branch current limits while maintaining computational tractability. The SOCP formulation preserves the principal electrical characteristics of the network and enables efficient enforcement of line loading restrictions during fault recovery and restoration processes.

3.2. Electric power system constraints

restrictions on AC current and safety limits are two examples of power system restrictions. With respect to online applications, the AC current limitations based on second-order cone programming are [15] in order to satisfy the computational efficiency requirement.

$$\begin{cases} P_{Gi} + P_{Ti} - P_{Li} = \sum_{j\in\delta(i)} P_{ij} \\ Q_{Gi} + Q_{Ti} - Q_{Li} = \sum_{j\in\delta(i)} Q_{ij} \\ P_{Li} = P_{Ci} + P_{Ei} \quad \forall i \in \Lambda \\ C_{ij}^2 + S_{ij}^2 = W_i W_j \\ \left\| \begin{matrix} C_{ij} \\ S_{ij} \end{matrix} \right\|_2 \leq \sqrt{W_i W_j} \end{cases} \tag{6}$$

where Λ is the set of grid nodes, $P_{\mathrm{T}i}$ and $Q_{\mathrm{T}i}$ are the active and reactive power generation of the gas unit at node i, $P_{\mathrm{L}i}$ and $Q_{\mathrm{L}i}$ are the active and reactive load power of node i, and $P_{\mathrm{G}i}, Q_{\mathrm{G}i}$ is the active and reactive power generation of the conventional unit at node i;

The node flow balance equations are formulated according to the mass conservation principle of natural gas networks. At each gas node, the total gas inflow together with local gas injections must be balanced by the total gas outflow and nodal demand, thereby ensuring physically feasible gas transportation throughout the network. P_{ij} and Q_{ij} are the active and reactive power flowing from node i to j, respectively; $P_{\mathrm{C}i}$ and $P_{\mathrm{E}i}$ are the active power utilized by the electric compressor and the active power of other electric loads at node i.

3.3. Restrictions on the electricity-gas coupling element

This research examines an electric-gas coupling device that comprises of a pressurization station and a gas unit. Among these, the gas unit serves as both a power generator and a gas load for the natural gas network. In the proposed framework, the GFT unit serves as a bidirectional energy coupling component and provides supplementary power support during fault recovery. In practical integrated energy systems, however, the operational characteristics of GFT units may exhibit significant temporal variations owing to fluctuating load demands, renewable energy intermittency, and dynamic network conditions. Its electric power can be thought of as being proportionate to the quantity of natural gas it uses. In the proposed framework, the P2G device utilizes surplus electrical energy to support natural gas recovery and improve system restoration capability. In practical integrated energy systems, however, renewable energy generation exhibits significant temporal variability and uncertainty. The energy conversion relationship for $m \in \gamma, i \in \Lambda$ fulfills, assuming that the gas generator at node i of the grid is a gas load at node m of the natural system.

$$P_{\mathrm{T}i} = \eta_{\mathrm{T}i,m} f_{\mathrm{T}m}^{\rm set} H_{\rm G} \tag{7}$$

where $H_{\rm G}$ is the natural gas's calorific value and $\eta_{\mathrm{T}i,m}$ is the gas generator's operational efficiency.

Assume for $m, n \in \gamma, i \in \Lambda$ that the grid node i's electric load is the electric pressurization station on the gas pipeline mn, and that its energy conversion relationship meets

$$\begin{cases} P_{\mathrm{C}i} = \eta_{\mathrm{C}i,mn} f_{\mathrm{C}mn,N_x^{mn}N_t^{mn}} \\ K_{\mathrm{C}mn} = \dfrac{p_{mn,N_x^{mn}j}}{p_{mn,0j}} \end{cases} \quad \forall j = 1,\ldots,N_t^{mn} \tag{8}$$

where P_{Ci} is the amount of electricity used at grid node i by the electric compressor; The pressurization ratio is f_{Cmn}, and the proportionality coefficient between the electric power used by the pipeline electric compressor and its prime mover drive flow is $\eta_{\mathrm{C}i,mn}$. For $m, n \in \gamma$, the pipeline mn pressurization station satisfies the safety limitations and boundary condition restrictions as follows:

$$\begin{cases} \underline{f}_{\mathrm{C}mn} \leq f_{\mathrm{C}mn,ij} \leq \bar{f}_{\mathrm{C}mn} \\ f_{\mathrm{C}mn,i0} = f_{\mathrm{C}mn,i}^0 \end{cases} \quad \forall i = 0,\ldots,N_x^{mn}, j = 1,\ldots,N_t^{mn} \tag{9}$$

where 0C, $f_{\mathrm{C}mn,i}^0$ is the mass flow rate of the pipeline mn pressurization station at the beginning moment t_0; $\bar{f}_{Cmn}$ and $\underline{f}_{Cmn}$ are the maximum and lower bounds of the mass flow rate, respectively. During the recovery process, the various energy resources operate in a coordinated manner to maximize restoration capability and improve system resilience. Distributed wind and photovoltaic generators primarily supply renewable electrical energy and reduce the dependence on conventional generation resources. Battery energy storage systems provide rapid charging and discharging support to compensate for renewable generation variability and satisfy short-term load requirements

4. Calculus analysis

This section verifies the efficacy of the methods presented in this paper using two examples: an IEEE 13-node system and a 6-node natural gas system. The optimization model is modeled by YALMIP, solved by CPLEX, and the final simulation results are achieved using MATLAB as the simulation programming environment. The optimization framework employed CPLEX owing to its computational efficiency and capability to solve large-scale optimization problems involving coupled electricity-gas system constraints. Although the present case studies demonstrated satisfactory computational performance, practical integrated energy systems may involve higher-dimensional decision spaces and increased operational uncertainties.

Figure 1 illustrates the topology of the integrated electricity-gas system, in which one GFT and one P2G device establish bidirectional coupling between the balanced IEEE 13-node electrical network and the 6-node natural gas network. The symbols E and G denote electrical and gas nodes, respectively, while brackets represent transmission lines and pipelines. The proposed optimization framework was implemented in YALMIP due to its flexibility in modelling coupled electricity-gas optimization problems with multiple operational constraints. Although the present study considered a medium-scale test system, the modelling framework is generic and can be extended to larger integrated energy networks containing additional coupling devices and operational variables.

Three scenarios were considered (see Table 2): Scenario 1 performed independent gas and electrical network recovery without coupling, Scenario 2 incorporated only GFT coupling, and Scenario 3 employed the proposed bidirectional GFT-P2G coupling strategy. The computation times were approximately 1 s for all scenarios, with Scenario 3 achieving the highest objective value (41489.14) due to maximum restoration of both electrical and gas loads.

The restoration process in all scenarios satisfied operational requirements through progressive network reconfiguration and load recovery actions. While Scenarios 1 and 2 primarily improved electrical load restoration using renewable sources and GFT support, Scenario 3 further restored additional gas loads through P2G-enabled bidirectional energy conversion, resulting in the highest objective

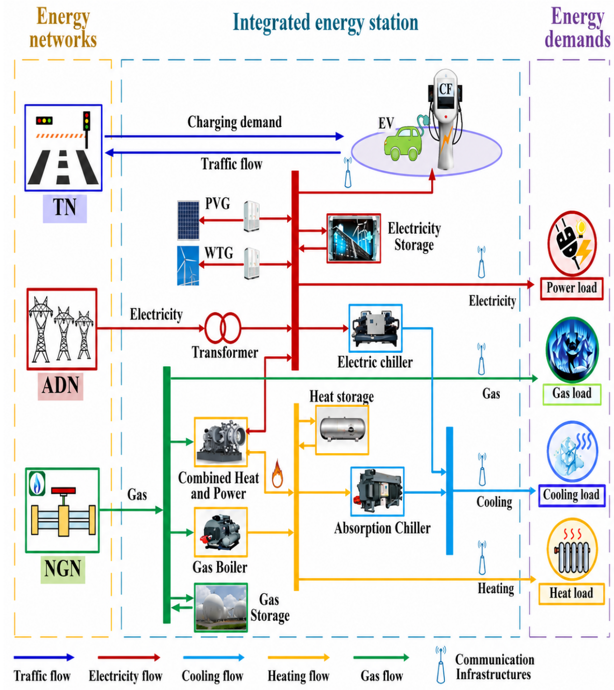

Fig. 1. 13-6: Integrated Energy System with Node for Electricity and Gas

function value is shown in Figure 2.

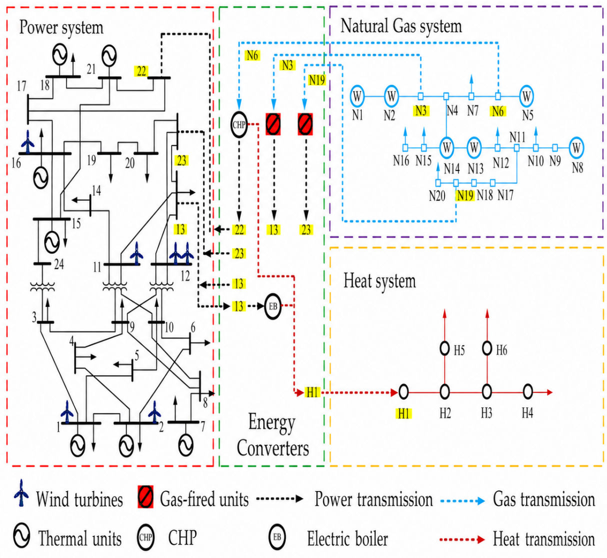

Fig. 2. Three scenarios of the recovery process

The amount of electrical load restored for Scenarios 2 and 3 is contrasted in Figure 3 at each stage of the restoration procedure. There is no restoration of load in the corresponding Scenario 3, which is a trade-off because additional restoration of natural gas network loads can be made in the subsequent steps of Scenario 3. As can be seen, the

Table 2. Values of the objective function for various circumstances

Scene	Objective function value	Recoverable capacity for electric loads	Capacity to recover gas loads	Calculation time/s
1	24521.16	18562.14	4548.24	0.85
2	38572.04	32458.58	4685.42	0.96
3	41489.14	28742.42	18574.85	1.14

amount of electrical load restored in Scenario 2 is 180 kW and 285 kW in Steps 3 and 6 of the restoration process, respectively.

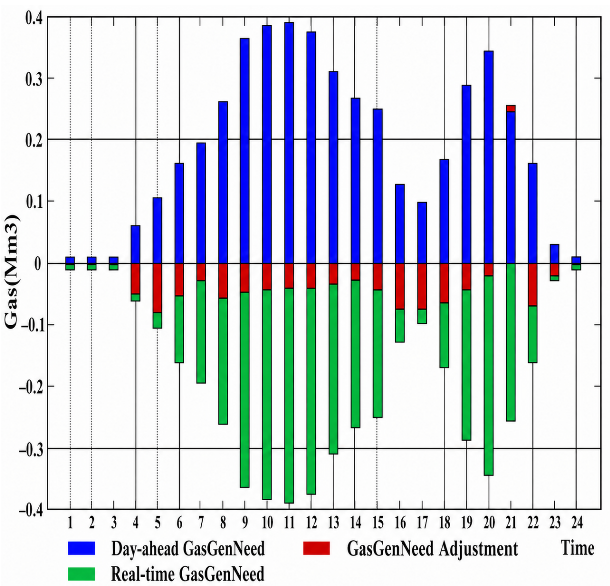

Fig. 3. Recovery process schematic illustration

Despite the vulnerable fault transfer topology formed during recovery, the proposed method maintained all node voltages within the safe operating range throughout the restoration process. All nodes were successfully restored, with the minimum voltage occurring at node E9 in Step 10, reaching 0.97 p.u is given in Figure 4.

Figure 5 illustrates the active power variations of storage batteries, GFT units, and P2G devices during recovery, showing their coordinated roles in maintaining network operating limits under changing topology and load conditions. The integration of wind and PV units in Steps 4 and 7 reduced battery output, while the GFT and P2G devices commenced operation in Steps 3 and 8, respectively.

Scenario 4 was configured as a control case of Scenario 3 with different line and pipeline faults to evaluate the robustness of the proposed bidirectional electricity-gas recovery strategy. Although its recovery objective function reached 95.75% of Scenario 3, the results demonstrate that the proposed method maintains effective restoration capability under various fault locations is given in Figure 6.

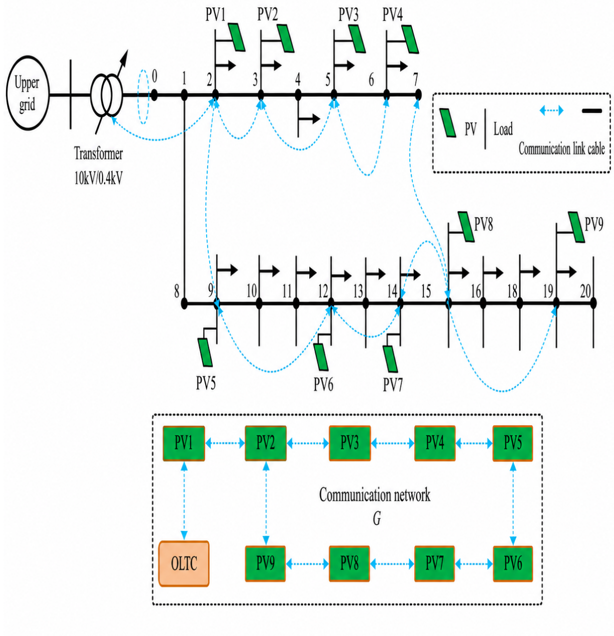

Fig. 4. Power network node voltage

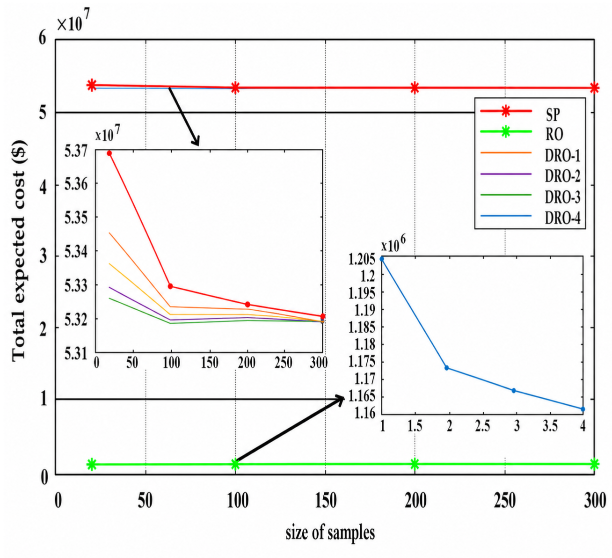

Fig. 5. Energy conversion equipment’ s output curve for the integrated electric-gas energy system

5. Conclusion

This work proposes an optimization technique for EGIES fault recovery using bi-directionally connected devices.

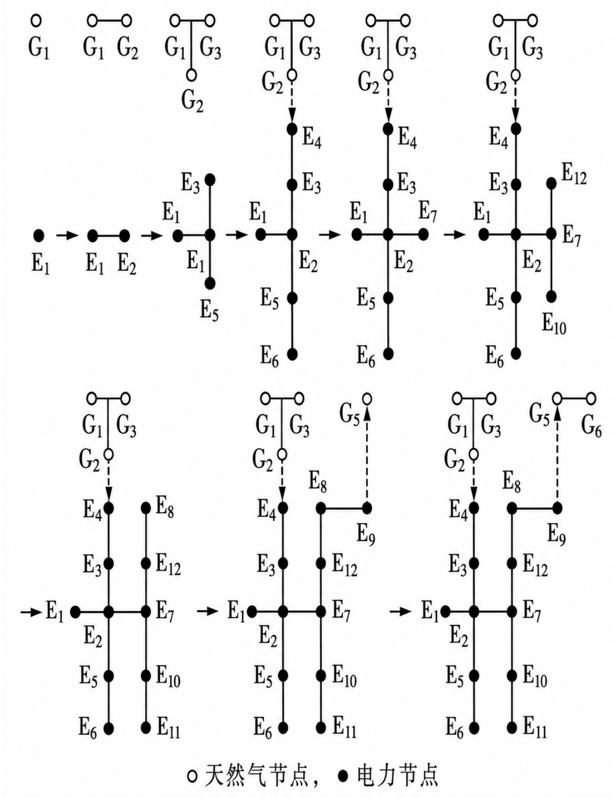

Fig. 6. A schematic representation of scene 4′ s recovery procedure

Through simulated studies on an IEEE 13-node power system and a 6-node natural gas system, the superiority and efficacy of the suggested method are confirmed. Three distinct recovery scenarios were set up in the simulation: independent recovery, recovery taking into account solely GFT coupling, and integrated recovery taking into account both GFT and P2G coupling. Based on the electric and natural gas load recovery being only 55.94% of Scenario 3, the results indicate that Scenario 1 (independent recovery) has the worst recovery effect. This is because no electric-gas coupling equipment is used in this scenario. When only GFT coupling is taken into account, Scenario 2 (which results in an overall recovery of 66.64% of Scenario 3) enhances electric load recovery by using GFT equipment to convert excess natural gas to electricity. However, due to downstream natural gas network breakdown, Scenario 2 is unable to recover. With an objective function value of 41,488.12, which is significantly better than the other scenarios, Scenario 3 (which takes into account both GFT and P2G coupling) maximizes the use of GFT and P2G equipment and achieves a two-way synergistic restoration of the natural gas and electric systems. It also has the largest total load restoration of gas and electricity.

Declaration

Data availability

No dataset was generated or analyzed in this study

Conflicts of interest

The authors declare that there are no conflicts of interest regarding the publication of this paper.

Funding statement

This research received no external funding.

Author contributions

Anjiang Liu: Conceptualization, methodology, modeling, writing – original draft.
Youzhuo Zheng: Data curation, software, validation.
Di Weng: Formal analysis, investigation.
Hengrong Zhang: Visualization, resources.
Xinhao Li: Supervision, writing – review and editing.

Ethical approval

This study does not involve human participants or animals, and therefore ethical approval is not required.

Consent to participate

Not applicable.

Consent for publication

Not applicable.

Competing interests

The authors declare that they have no competing interests.

Code availability

The code used in this study (MATLAB/YALMIP models and CPLEX optimization scripts) is available from the corresponding author upon reasonable request.

Acknowledgement

The authors would like to thank the Electric Power Research Institute, Guizhou Power Grid Co., Ltd., for providing technical support and resources for this research.

References

[1] N. M. Sami and M. Naeini, (2024) *"Machine Learning Applications in Cascading Failure Analysis in Power Systems: A Review"* **Electric Power Systems Research** ***232***: 110415. DOI: 10.1016/j.epsr.2024.110415.

[2] X. Fu et al., (2023) *"Tolerance Analysis of Cyber-Manufacturing Systems to Cascading Failures"* **ACM Transactions on Internet Technology** ***23***(4): 1–23. DOI: 10.1145/3579847.

[3] B. Rolf et al., (2023) *"A Review on Reinforcement Learning Algorithms and Applications in Supply Chain Management"* **International Journal of Production Research** ***61***(20): 7151–7179. DOI: 10.1080/00207543.2022.2140221.

[4] L. He et al., (2023) *"Research Progress of Microwave Plasma Ignition and Assisted Combustion"* **Chinese Journal of Aeronautics** ***36***(12): 53–76. DOI: 10.1016/j.cja.2023.04.029.

[5] J. P. Futalef et al. "An Importance Function to Generate Scenarios for Training a Grey-Box Model for the Computational Risk Assessment of Cyber-Physical Systems". In: *Proceedings of the 33rd European Safety and Reliability Conference (ESREL 2023)*. 2023, 2130–2137. DOI: 10.3850/978-981-18-8071-1_P684-cd.

[6] Y. Li et al., (2023) *"Dynamic Prediction and Driving Factors of Carbon Emission in Beijing, China, under Carbon Neutrality Targets"* **Atmosphere** ***14***(5): 798. DOI: 10.3390/atmos14050798.

[7] S. Ghorbany, S. Yousefi, and E. Noorzai, (2024) *"Evaluating and Optimizing Performance of Public–Private Partnership Projects Using Copula Bayesian Network"* **Engineering, Construction and Architectural Management** ***31***(1): 290–323. DOI: 10.1108/ECAM-05-2022-0492.

[8] J. Fang, D. Liu, and K. T. Chi. "Predicting Onset Time of Cascading Failure in Power Systems Using a Neural Network-Based Classifier". In: *Proceedings of the IEEE International Symposium on Circuits and Systems (ISCAS)*. 2022, 3522–3526. DOI: 10.1109/ISCAS48785.2022.9937800.

[9] A. Varbella, B. Gjorgiev, and G. Sansavini, (2023) *"Geometric Deep Learning for Online Prediction of Cascading Failures in Power Grids"* **Reliability Engineering & System Safety** ***237***: 109341. DOI: 10.1016/j.ress.2023.109341.

[10] S. He et al., (2022) *"Fast Identification of Vulnerable Set for Cascading Failure Analysis in Power Grid"* **IEEE Transactions on Industrial Informatics** ***19***(4): 5645–5655. DOI: 10.1109/TII.2022.3202917.

[11] X. Li, T. Pan, and K. Pan, (2022) *"Identification of Key Components after Unintentional Failures for Cascading Failure Protection"* **IEEE Transactions on Network Science and Engineering** ***10***(2): 1003–1014. DOI: 10.1109/TNSE.2022.3225459.

[12] R. Feng, (2024) *"Multi-Scale Deep Learning-Based University Financial System: Hardware Design and Database Integration"* **Journal of Combinatorial Mathematics and Combinatorial Computing** ***120***: 337–344. DOI: 10.61091/jcmcc120-30.

[13] Z. Guo et al., (2023) *"A Review on Simulation Models of Cascading Failures in Power Systems"* **iEnergy** **2**(4): 284–296. DOI: 10.23919/IEN.2023.0039.

[14] Y. Liu, T. Wang, and J. Guo, (2022) *"Identification of Vulnerable Branches Considering Spatiotemporal Characteristics of Cascading Failure Propagation"* **Energy Reports** ***8***: 7908–7916. DOI: 10.1016/j.egyr.2022.06.016.

[15] S. Lonapalawong et al., (2022) *"Interpreting the Vulnerability of Power Systems in Cascading Failures Using Multi-Graph Convolutional Networks"* **Frontiers of Information Technology & Electronic Engineering** ***23***(12): 1848–1861. DOI: 10.1631/FITEE.2200035.